



Data-Driven Self-sensing Technique for Active Magnetic Bearing

Seong Jong Yoo¹ · Sinyoung Kim² · Kwang-Hwi Cho³ · Hyeong-Joon Ahn⁴

Received: 29 July 2020 / Revised: 26 March 2021 / Accepted: 13 April 2021 / Published online: 4 May 2021
© Korean Society for Precision Engineering 2021

Abstract

In the last two decades, soft sensors proved themselves as a valuable alternative to the physical sensor for gathering critical process information. A self-sensing technique for the magnetic bearing is considered as a soft sensor since the object position is estimated from the current signal of the electromagnet. Self-sensing techniques developed so far are the model-driven soft sensors. This paper presents a data-driven self-sensing technique to compensate for the nonlinear characteristic of the electromagnet. First, model-driven self-sensing techniques and their problems are reviewed. Then, data-driven self-sensing technique using recurrent neural network (RNN) is proposed to compensate for the nonlinear characteristics. Both the position control and self-sensing with the RNN are implemented in a single digital signal processor. The effectiveness of the proposed method is experimentally verified by comparison with the current slope method. Both estimation errors during initial levitation and jitter after levitation are reduced by 90% and 36%, respectively. Estimation error with 2 Hz sine wave is improved by 65.9%, while jitter during self-sensing levitation is cut down to 26.8%.

Keywords Data-driven sensor · Self-sensing · Active magnetic bearing · RNN

List of symbols

A_g	Cross-section area of E core	V_{dc}	DC link voltage
a	Area ratio of E core	W	RNN layer weight
b	RNN bias	x	Air gap
h_i	RNN i th hidden layer value	x_0	Nominal air gap
H	Unit step function	x_n	Discretized air gap
I	Current	\hat{x}_n	Estimated air gap
L	Coil inductance	X_i	RNN i th input value
N_c	Number of PWM period	β	Voltage coefficient
R	Coil resistance	γ	PWM duty cycle
T_S	PWM switching period	μ_0	Magnetic permeability of air
u	PWM voltage to drive the coil	τ	Time constant of coil
U	RNN input weight		

✉ Hyeong-Joon Ahn
ahj123@ssu.ac.kr

¹ Department of Mechanical Engineering, Graduate School, Soongsil University, 396, Sangdo-ro, Dongjak-gu, Seoul 06978, Republic of Korea

² Department of Bioinformatics, Soongsil University, 396, Sangdo-ro, Dongjak-gu, Seoul 06978, Republic of Korea

³ School of Systems Biomedical Science, Soongsil University, 396, Sangdo-ro, Dongjak-gu, Seoul 06978, Republic of Korea

⁴ School of Mechanical Engineering, Soongsil University, 396, Sangdo-ro, Dongjak-gu, Seoul 06978, Republic of Korea

1 Introduction

In the last two decades, soft sensors proved themselves as a valuable alternative to the physical sensor for gathering critical process information. Predictive or virtual models are built based on the large amounts of data being measured and stored in the process industry, which are called soft sensors. This is a combination of the words “software” to compose of computer programs, and “sensors” to deliver similar information with hardware sensors [1–3].

Soft sensors are classified into two categories: model and data-driven soft sensors [4]. Model-driven soft sensors is commonly based on the first principle under ideal

conditions. On the other hand, data-driven models apply statistical techniques to predict the value of interest. Besides, the data-driven soft sensor describes the true process condition better than the model-driven soft sensor since all data are measured within the real process.

The self-sensing technique for the magnetic bearing is considered a soft sensor since the object position is estimated from the current signal of the electromagnet [5]. Although a gap sensor is an essential element to firmly support an object, the position sensor increases the cost and size as well as causes difficult engineering or non-collocation problem. Different self-sensing approaches for magnetic bearing have been studied to replace the physical position sensor with a virtual software sensor or self-sensing technique.

Self-sensing techniques developed so far are the model-driven soft sensors [6–16]. Self-sensing techniques rely on the circuit equation of the electromagnet derived under the ideal condition and the nonlinear characteristic of the electromagnet is one of the most challenging problems for self-sensing technique [9].

This paper presents a data-driven self-sensing technique to compensate for the nonlinear characteristic of the electromagnet. First, model-driven self-sensing techniques and their problems are reviewed briefly. Then, data-driven self-sensing technique using RNN is proposed to compensate for the nonlinear characteristics. The effectiveness of the proposed method is experimentally verified by comparison with the current slope method.

2 Self-sensing for AMB (Active Magnetic Bearing)

AMB is to support the object without any contact using electromagnetic actuators and the feature of non-contact allows lubrication-free, high-speed operation, and easy maintenance. Therefore, AMBs have been applied to vacuum techniques, turbomachinery, electric drives, space and physics fields [17–19].

AMB consists of an electromagnet, an object to be suspended, a sensor, and a controller, as shown in Fig. 1. The position or gap sensor is an essential element for stably controlling the position of objects. However, the position sensor not only increases the hardware cost and size but also causes non-collocation problems, which indicates that the sensor and the actuator are not located at the same placement.

Researchers have studied sensorless or self-sensing magnetic bearing by using an electromagnetic actuator as a sensor. In detail, the target movement changes the inductance of the electromagnetic actuator and results in a variation of the current signal due to the driving voltage. The target position can be estimated by measuring the current signal according to the driving voltage. Previous studies of self-sensing

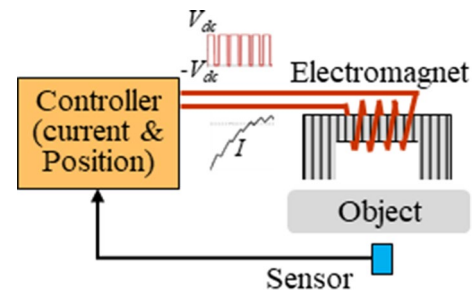


Fig. 1 Typical block diagram of active magnetic bearings

magnetic bearings are classified into three main methods. The first one is last method is more accurate and simpler than the other methods, it the state observer. In this method, the position is estimated with a state observer based on control theory [6–8, 20]. However, this method does not show either adequate accuracy or robustness even a little further from the operating point. The second one is the signal injection method. A high-frequency voltage signal is injected into the electromagnetic actuator and the current signal of the actuator is measured to estimate the target position through a demodulation circuit [9]. However, the desired performance can hardly be achieved due to the trade-off between the bandwidth and the accuracy of the position estimation. The final one is the parameter estimation method. The position is estimated from the current ripple or slope due to PWM voltage [10–13, 21]. The PWM voltage is very high frequency and has considerable amplitude to overcome the drawback of the high-frequency signal injection method. Although the still has estimation errors caused by non-linear properties and PWM duty cycle [15, 16].

3 Data-Driven Self-sensing

3.1 Model-Based Self-sensing Using Current Slope

If the coil of an electromagnet is driven by PWM voltage, the current ripple generated during switching is dependent on the inductance of the coil. Since the coil inductance is inversely proportional to the air gap, the air gap of the electromagnet can be estimated using the magnitude of the current ripple of the PWM [9]. Since the amplitude of the current ripple also highly depends on the PWM duty cycle, we need to compensate the effect of PWM duty cycle for accurate estimation of the air gap.

The slope of the current ripple was also used to estimate the air gap instead of the magnitude to reduce the effect of the PWM duty cycle [16]. The current slope is usually measured several times with a separate embedded device such as FPGA and estimated with the least square method. The circuit equation for the current can be expressed with

Eq. (1). Here, x is air gap variation, x_0 is a nominal air gap, u is PWM voltage to drive the coil, R is the resistance of the coil and I is coil current.

$$\dot{i} = \dot{x} \frac{I}{x + x_0} + \frac{(x + x_0)}{\beta} (u - RI) \tag{1}$$

$$\dot{i} = \frac{(x_n - x_{n-1})}{T_s} \left(\frac{I}{x_n + x_0} \right) + \frac{(x_n + x_0) \mu_0 A_g N^2}{1 + a} (V_{dc} - RI) \tag{2}$$

$$\hat{x}_n = \frac{I \hat{x}_{n-1} T_s \dot{i} x_0 - T_s \beta x_0^2 (V_{dc} - RI)}{I + 2\beta T_s x_0 (V_{dc} - RI) - T_s \dot{i}} \tag{3}$$

The approximate current profile due to bipolar PWM is shown in Fig. 2. Here, T_s is the sampling time. Current at several points during a given cycle time is measured to calculate the slope of the current ripple. Equation (1) can be discretized as Eq. (2) considering the forward difference of x and $u = V_{dc}$ during the current measurement. Here, T_s is the PWM switching period and V_{dc} is the voltage of the DC supplier. The air gap can be estimated from the measured current slope as shown in Eq. (3). Here, $(1 + x_n/x_0)^2 \approx (1 + 2x_n/x_0)$ considering $x_n \ll x_0$. As shown in Eq. (3), the nominal gap, current, and current slope are the main variables. When the average current increases or the current slope decreases, the estimated gap increases.

The non-linear relationship between the PWM current slope and the PWM duty ratio under various air gaps is measured and shown in Fig. 3. The current slopes are measured as increasing PWM duty up to 5 A coil current with a constant air gap. Although the current slope theoretically does not depend on the PWM duty cycle [15], PWM duty cycle has a large effect on the current slope under the small air gap, which may cause considerable estimation error, especially during an initial levitation. The voltage can be expressed as Eq. (4) considering bipolar PWM and duty cycle γ .

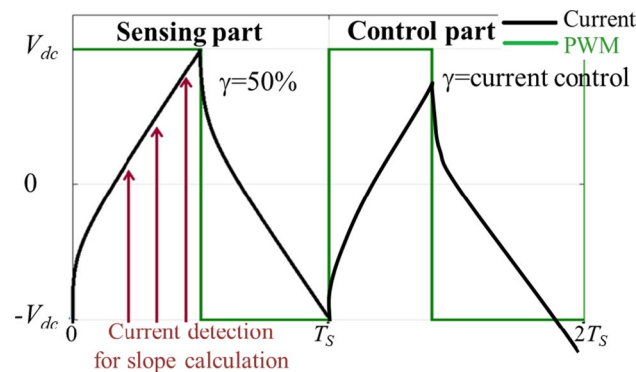


Fig. 2 Bipolar PWM and current slope estimation

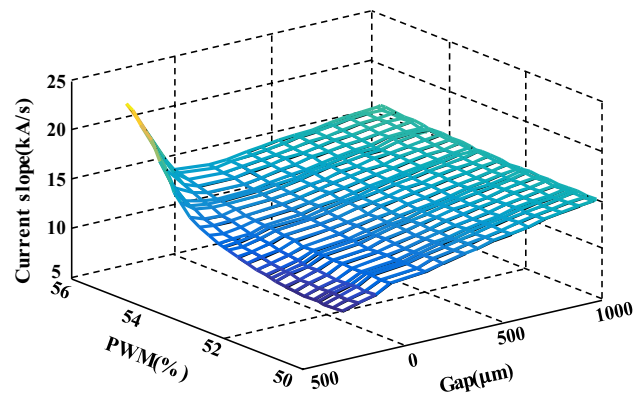


Fig. 3 Non-linear relationship between PWM current slope and PWM duty under various air gaps

The current in one PWM cycle can be expressed with Eq. (5). Here, $H(t)$ is the unit step function. Differentiating Eq. (5) and considering constant voltage (V_{dc}) during measuring the current, the current slope does not depend on the PWM duty cycle, as shown in Eq. (6). In the case of a 50% PWM duty cycle (zero voltage command), the current slope is nearly proportional to the air gap, as shown in Fig. 3.

$$V(t) = \begin{cases} V_{dc} & (N_c T_s \leq t < N_c T_s + \gamma T_s) \\ -V_{dc} & (N_c T_s + \gamma T_s < t \leq (N_c + 1) T_s) \end{cases} \tag{4}$$

$$I(t) = e^{-\tau t} I(0) + \frac{V_{dc}}{R} \left((1 - e^{-\tau t}) - 2(1 - e^{-\tau(t-\gamma T_s)}) H(t - \gamma T_s) + (1 - e^{-\tau(t-T_s)}) H(t - T_s) \right) \tag{5}$$

$$\dot{i} \left(\frac{T_s}{4} \right) = \left(\frac{V_{dc}}{L} - \frac{R}{L} I(0) \right) e^{-\tau T_s/4} \tag{6}$$

Since the initial current or $I(0)$ of Eq. (5) within a given cycle time is closely related to the PWM duty cycle, the current slope must depend on the PWM duty cycle. Besides, non-linear characteristics such as eddy current, magnetic flux leakage, and saturation affect the estimation error of the air gap and result in degrading robustness of the position control. Furthermore, the initial current is no longer a constant value due to continuously varying PWM during the position control of AMB, and the nonlinearity becomes stronger. The higher PWM duty cycle and smaller air gap result in a severe non-linear relationship between the current slope, PWM duty, and air gap, which usually happens during the initial levitation. The high flux density due to the large current and small air gap makes

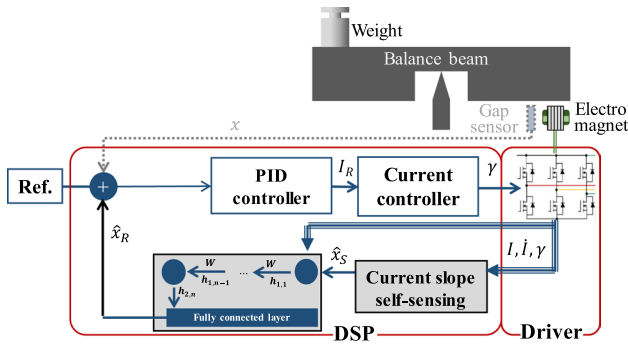


Fig. 4 Block diagram of the data-driven approach for self-sensing

Table 1 Training result for various activation functions

Activation function	R^2	Q^2
Hyperbolic tangent	0.9914	0.9710
ReLU	0.9731	0.8590
Sigmoid	0.9826	0.9361

the electromagnet operate in the nonlinear part of the BH curve.

3.2 Data-Driven Approach for Self-sensing

A schematic diagram of the data-driven approach for the self-sensing is shown in Fig. 4. There are two estimated air gaps: one is calculated using the model-based method (\hat{x}_S), and the other is an output of the RNN model (\hat{x}_R). Due to the physical limitation of digital signal processor (DSP), deep and complex neural network is not suitable for our application. Hence, we adopted a simple vanilla structure of RNN, consisting of one or two layers and three to seven sequential lengths and hidden dimensions. First, we estimate the air gap using the model-based method of Eq. (3). Then, RNN compensates for the nonlinearity of the estimated air gap. We used not only the estimated gap of the model-based method but also average current, PWM duty, and current slope (current change during one PWM cycle) as input for RNN. Besides, a fully-connected layer is used to integrate all features of the input for RNN.

After various activation functions are tested as shown in Table 1, the hyperbolic tangent function is finally employed as an activation function. Here, R^2 is the training score and Q^2 is the test score. The square sum of the estimation error of the air gap is used as the cost function. We employed the Adam optimization algorithm and set a 0.01 learning rate to update the weight. Besides, we used the dropout technique to avoid over-fitting.

Sine wave tracking experiment is used for training data of RNN, while the initial levitation experiment is used as test

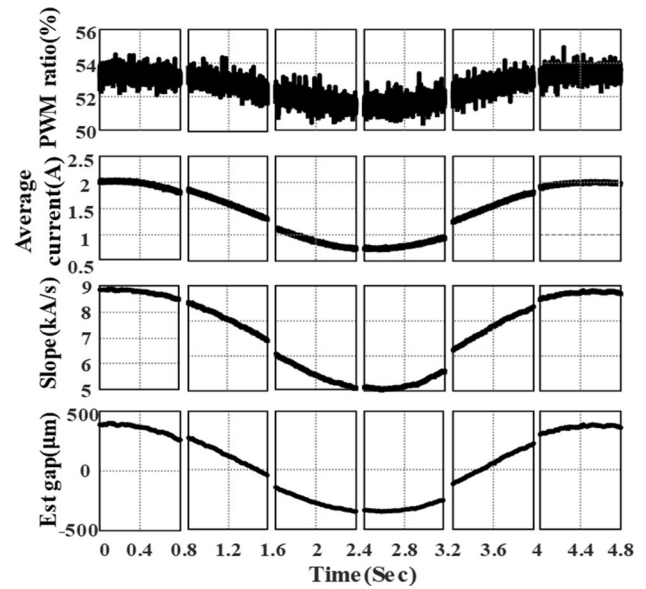


Fig. 5 Training data for one batch

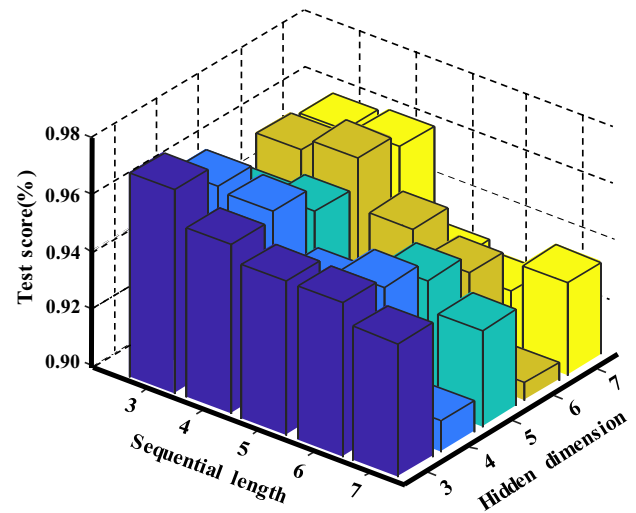


Fig. 6 Training result for each RNN model

data. Training data is 0.2 Hz sine wave with an amplitude of 400 μm , which is slightly less than the nominal air gap. While learning the model, we use 6 sizes of batch training. Each batch consists of 4000 data of partial sine wave, as shown in Fig. 5. Test data is the initial levitation from -500 to $0 \mu\text{m}$ or the balanced state, which is one of the most important behaviors of magnetic levitation systems. As the hyperparameters such as the number of hidden dimensions and sequential length are adjusted, training is performed 10,000 times and the result is shown in Fig. 6. RNN with one layer, three hidden dimensions, and three sequential lengths show the best test score. Besides, the training result

Table 2 Training results for various models and hyperparameters

Model	RNN	LSTM	LSTM
Layer	1	1	2
Sequential length	3	5	7
Hidden dimension	3	5	5
R^2	0.9914	0.9964	0.9895
Q^2	0.9710	0.9186	0.8800

Table 3 Specifications for the AMB system

Parameter	Value	Parameter	Value
Weight	1 kg	Air gap	- 0.5 to 0.5 mm
Weight location	144.5 mm	Inertia	0.181 kg m ²
Electromagnet location	156.6 mm	Coil turns	118

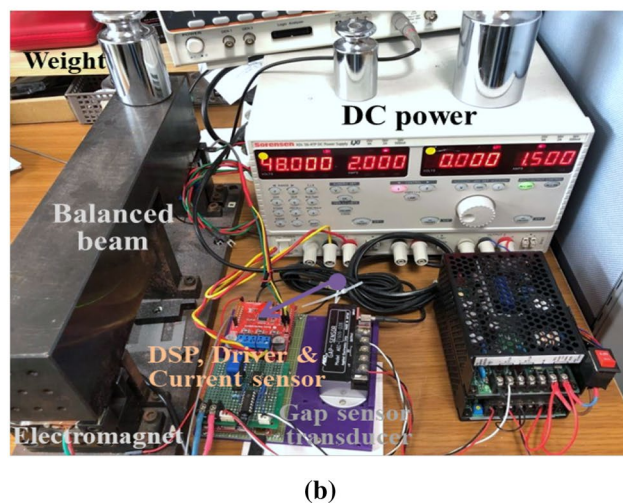
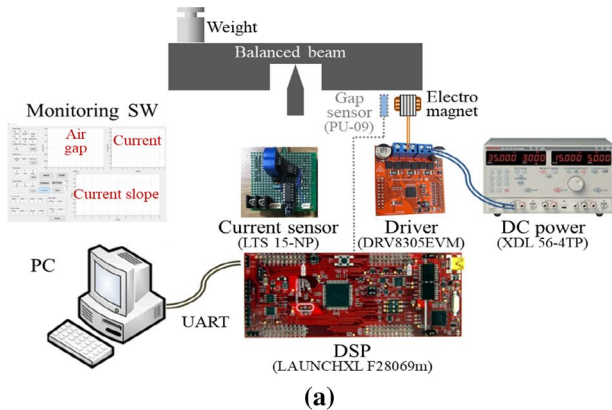


Fig. 7 Block diagram of experimental set-up and device. **a** Block diagram, **b** experimental device

of LSTM (long short-term memory) is compared with that of RNN in Table 2. The RNN model reported a higher test score than any other LSTM model since the states of AMB changes rapidly during the initial levitation and the short-term memory of the LSTM is no longer critical for the performance.

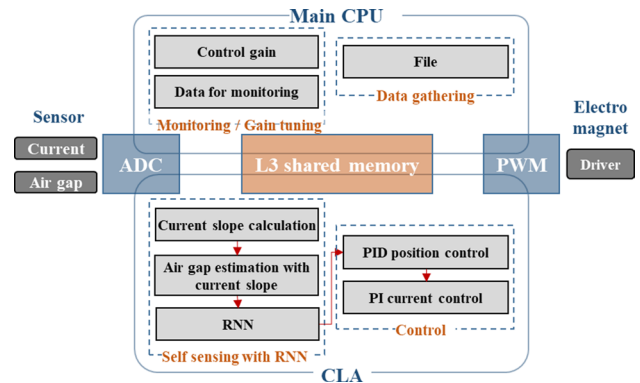


Fig. 8 DSP structure for control and self-sensing

4 Experiment

4.1 Experimental Equipment

The experimental set-up of the SISO AMB system using self-sensing with RNN is shown in Fig. 7. One DOF SISO AMB system consists of a balanced beam supported with pivot bearing, an electromagnetic actuator on one side, and the weight on the other side. Parameters of the SISO AMB system are summarized in Table 3.

Electronics for self-sensing consists of a DSP (Launchpad-F28069M), 3 phase motor driver (BOOSTXL-DRV8305EVM), In-house current sensor circuit, power supply (48 V), and PC. Online monitoring and gain tuning programs are built via UART. The average current is measured with a shunt resistor in the 3-phase motor driver while the current slope is calculated with a current sensor (LEM, LTS 15-NP). We use a 0.007 Ω resistor with a differential connection in the power driver (DRV8305) to sense the average current. The current ripple is differentially amplified by 40 V/A around 1.65 V and digitized with a built-in 12-bit ADC of DSP [22]. A reference gap sensor (AEC, PU-09) is used to evaluate the performance of the self-sensing with RNN.

4.2 Implementation of RNN with DSP

Self-sensing with RNN is implemented in CLA (control law accelerator) together with position and current control, as

shown in Fig. 8. Based on Eq. (3), the air gap is firstly estimated using the current slope and the RNN compensates the nonlinearity of the estimated air gap. Then, PID position and PI current controls are used to levitate the balanced beam. Training and model parameters are determined off-line using python and TensorFlow. Then, weights for the neural network are extracted and the RNN model is implemented based on hard coding, as shown in Algorithm 1 below. Since the CLA provides efficient floating-point operation in hardware, the RNN that has high computation cost is realized in CLA so that the control and self-sensing can be completed in a sample time.

Algorithm 1 : 1 layer RNN model

Input	Current, PWM duty, current slope, and estimated air gap with current slope
1 :	Update the input matrix // Calculate the first sequence node
2 :	$h_1 = f(X_1 * U)$ // Calculate other sequence nodes
3 :	for $i = 2 \dots$ sequential length do
4 :	$h_i = f(X_i * U + h_{i-1} * W + b)$
5 :	end for // Calculate fully connected layer
6 :	Est gap = $H_{\text{sequential length}} * FW + Fb$
Output	Est gap

4.3 Result

Comparison of self-sensing with current slope and RNN during initial levitation is shown in Fig. 9. At the very early stage of initial levitation, self-sensing with the current slope has a peak estimation error of 400 μm while that with RNN has just an estimation error of 40 μm (90% improvement). Besides, self-sensing with RNN has a jitter of 9 μm , which is a 36% improvement compared with 14 μm of the previous method using the current slope.

Sine wave tracking experiments with self-sensing using current slope and RNN are shown in Fig. 10 (2 Hz).

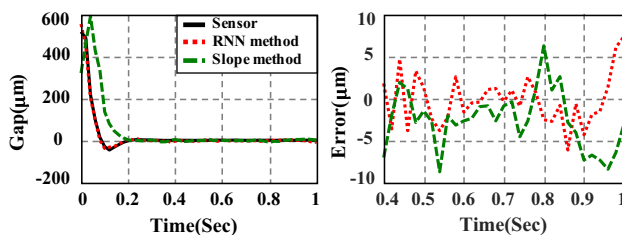


Fig. 9 Air gap estimation of RNN and current slope methods during initial levitation **a** estimation performance, **b** estimation errors

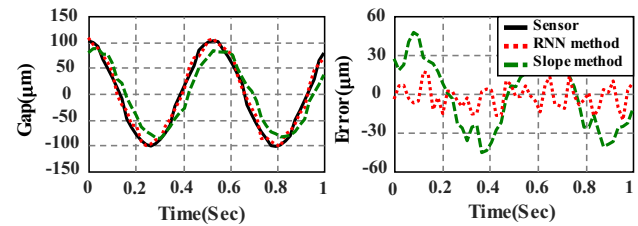


Fig. 10 Air gap estimation of RNN and current slope methods under 2 Hz sine wave reference. **a** Results, **b** errors

Self-sensing with the current slope has a 51 μm peak tracking error and very large phase delay while that with RNN has 17.55 μm peak tracking error (65.9% improvement) and very small phase delay.

The balance beam is levitated with two self-sensing methods and their performances are compared in Fig. 11. Levitation jitter with current slope is 265.3 μm while that with RNN is 194.3 μm (26.8% improvement).

5 Conclusions

This paper presents a data-driven self-sensing technique to compensate for the nonlinear characteristic of the electromagnet. First, model-driven self-sensing techniques and their problems are reviewed briefly. Then, data-driven self-sensing technique using RNN (recurrent neural network) is proposed to compensate for the nonlinear characteristics. Both the position control and self-sensing with the RNN are implemented in a single digital signal processor (DSP). The effectiveness of the proposed method is experimentally verified by comparison with the current slope method. Both estimation errors during initial levitation and jitter after levitation are reduced by 90% and 36%, respectively. Estimation error with 2 Hz sine wave is improved by 65.9% while jitter during self-sensing levitation is cut down to 26.8%.

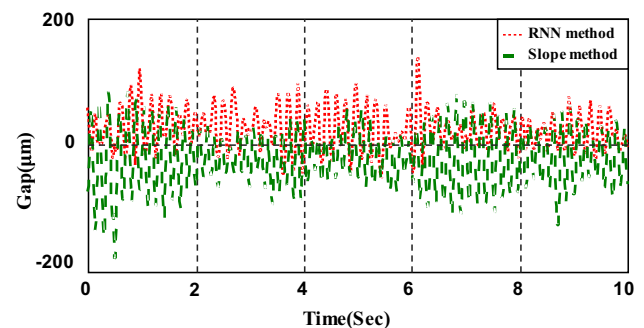


Fig. 11 Measured air gap during sensorless control with RNN and current slope methods under step reference

Acknowledgements This paper was supported by the Korea Institute of Advancement of Technology (KIAT) Grant funded by the Korea Government (MOTIE) (P0006915, Korea-China Joint R&D Project) and by the Soongsil University Research Fund of 2018.

References

- Kadlec, P., Gabrys, B., & Strandt, S. (2009). Data-driven soft sensors in the process industry. *Computers and Chemical Engineering*, 33, 795–814
- Gu, H., Zhu, H., & Hua, Y. (2018). Soft Sensing Modeling of Magnetic Suspension Rotor Displacements Based on Continuous Hidden Markov Model. *IEEE Transactions on Applied Superconductivity*, 28(3), 1–5
- Liu, T., Zhu, H., Wu, M., & Zhang, W. (2020). Rotor Displacement Self-Sensing Method for Six-Pole Radial Hybrid Magnetic Bearing Using Mixed-Kernel Fuzzy Support Vector Machine. *IEEE Transactions on Applied Superconductivity*, 30(4), 1–4
- Kadlec, P., & Gabrys, B. (2009). Soft sensors: Where are we and what are the current and future challenges? *IFAC Proceedings*, 42(19), 572–577
- Sun, Z., Zhao, J., Shi, Z., & Yu, S. (2014). Soft sensing of magnetic bearing system based on support vector regression and extended Kalman filter. *Mechatronics*, 24, 186–197
- Vischer, D., & Bleuler, H. (1993). Self-sensing active magnetic levitation. *IEEE Transactions on Magnetics*, 29(2), 1276–1281
- Morse, N., Smith, R., Paden, B., & Antaki, J. (1998). Position sensed and self-sensing magnetic bearing configurations and associated robustness limitations. In *Proceedings of the 37th IEEE conference on decision and control, Tampa* (Vol. 3, pp. 2599–2604).
- Thibeault, N., & Smith, R. (2002). Magnetic bearing measurement configurations and associated robustness and performance limitations. *Journal of Dynamic Systems, Measurement and Control*, 124, 589–598
- Park, Y. H., Han, D. C., Park, I. H., Ahn, H. J., & Jang, D. Y. (2008). A self-sensing technology of active magnetic bearings using a phase modulation algorithm based on a high frequency voltage injection method. *Journal of Mechanical Science and Technology*, 22(9), 1757–1764
- Noh, M. D., & Maslen, E. H. (1997). Self-sensing magnetic bearings using parameter estimation. *IEEE Transactions on Instrumentation and Measurement*, 46(1), 45–50
- García, P., Guerrero, J. M., El-Sayed, I., Briz, F., & Reigosa, D. (2010). Carrier signal injection alternatives for sensorless control of active magnetic bearings. In *First symposium on sensorless control for electrical drives, Padova* (pp. 78–85).
- Schammas, A., Herzog, R., Buhler, P., & Bleuler, H. (2005). New results for self-sensing active magnetic bearings using modulation approach. *IEEE Transactions on Control Systems Technology*, 13(4), 509–516
- Niemann, A. C., Van Schoor, G., & Du Rand, C. P. (2013). A self-sensing active magnetic bearing based on a direct current measurement approach. *Sensors*, 13(9), 12149–12165
- Glück, T., Kemmetmüller, W., Tump, C., & Kugi, A. (2011). A novel robust position estimator for self-sensing magnetic levitation systems based on least squares identification. *Control Engineering Practice*, 19(2), 146–157
- Hofer, M., Nenning, T., Hutterer, M., & Schrödl, M. (2014). Current slope measurement strategies for sensorless control of a three phase radial active magnetic bearing. In *Proceedings of the 22nd international conference on magnetically levitated systems and linear drives*.
- Wang, J. (2016). *The current slope based position estimation for self-sensing magnetic bearings*. Shaker Verlag.
- Schweitzer, G., Bleuler, H., & Traxler, A. (1994). *Active magnetic bearings: Basics, properties and applications of active magnetic bearings*. Vdf Hochschulverlag AG an der ETH Zürich.
- Schweitzer, G., & Maslen, E. (2009). *Magnetic bearings: Theory design and application to rotating machinery*. Springer.
- Asama, J., Asami, T., Imakawa, T., Chiba, A., Nakajima, A., & Rahman, M. A. (2011). Effects of permanent-magnet passive magnetic bearing on a two-axis actively regulated low-speed bearingless motor. *IEEE Transactions on Energy Conversion*, 26(1), 46–54
- Bobtsov, A. A., Pyrkin, A. A., Ortega, R. S., & Vedyakov A. A. (2018). A state observer for sensorless control of magnetic levitation systems. *Automatica*, 97, 263–270
- Jiang, Y., Wang, K., Sun M., & Xie, J. (2019). Displacement Self-Sensing Method for AMB-Rotor Systems Using Current Ripple Demodulations Combined With PWM Command Signals. *IEEE Sensors*, 19(14), 5460–5469
- Texas Instruments. (2015). BOOSTXL-DRV8305EVM User's Guide. <https://www.ti.com/lit/pdf/slvuai8>.

Publisher's Note Springer Nature remains neutral with regard to jurisdictional claims in published maps and institutional affiliations.



Seong Jong Yoo received the B.S. and M.S. degrees in mechanical engineering from Soongsil University, Seoul, Korea in 2017 and 2019, respectively. He is currently working at Korea Institute of Science and Technology as a researcher. His interest include system control, mechatronics and signal processing.



Sinyoung Kim received the B.S. degree in civil engineering from Konkuk University, Seoul, Korea in 2016 and the M.S. degree in Department of Bioinformatics from Soongsil University, Seoul, Korea in 2018. She is currently working at AmorePacific as a data analyst.



Kwang-Hwi Cho received the B.S. and M.S. degrees in chemistry from Soongsil University, Seoul, Korea in 1989 and 1991, respectively, and the Ph.D. Degree in computational chemistry from Cornell university, Ithaca, NY, USA in 2000. After working as a postdoctoral fellow in NIH, MD, USA for two years, he became a professor at the School of Systems Biomedical Science, Soongsil University in 2003.



Hyeong-Joon Ahn received B.S., M.S. and Ph.D. degrees from Seoul National University, Korea in 1995, 1997 and 2001, respectively. He was research associate in University of Virginia, 2002. He is currently a professor at School of Mechanical Eng., Soongsil University. His research interests include mechatronics, sensors, actuators, control and precision machine design.